JOURNAL OF Applied Polymer SCIENCE

Deformation and Fracture Behaviors of Vinylester/Fly Ash Composites

A. Stocchi,[1] E. Rodríguez,[1] A. Vázquez,[1,2] C. Bernal[3]

[1]Materials Science and Technology Research Institute (INTEMA), University of Mar del Plata—National Research Council (CONICET), B7608FDQ Mar del Plata, Argentina

[2]Polymers and Composite Materials Group, INTECIN (UBA-CONICET), Construction Department, Engineering Faculty, University of Buenos Aires, C1127AAR Buenos Aires, Argentina

[3]Advanced Materials Group (GMA), INTECIN (UBA-CONICET), Department of Mechanical Engineering, Engineering Faculty, University of Buenos Aires, C1063ACV Buenos Aires, Argentina

Correspondence to: C. Bernal (E-mail: cbernal@fi.uba.ar)

ABSTRACT: In this work, the deformation and fracture behaviors of a commercial vinylester resin reinforced with fly ash were investigated. Tensile, compressive, and fracture tests were performed on the matrix and the composites with different ash content. Most composites exhibited improved stiffness, tensile strength, and fracture properties in comparison to the vinylester matrix. From scanning electron microscopic analysis of fracture surfaces, the toughening mechanisms of crack pinning, crack deflection, particle debonding, and localized shear yielding were identified. In addition, the dependence of tensile and compressive modulus and fracture energy toward ash content was adequately fitted by simple models available in the literature. From the results of these models and energy-dispersive X-ray spectroscopy analysis, some interaction between vinylester and ash seemed to exist. © 2012 Wiley Periodicals, Inc. J. Appl. Polym. Sci. 000: 000–000, 2012

KEYWORDS: composites; mechanical properties; fracture

Received 7 September 2011; accepted 22 June 2012; published online
DOI: 10.1002/app.38305

INTRODUCTION

There is an increasing current interest of technical and scientific community to obtain new materials with improved properties and processability at relatively low cost. This is commonly achieved through the incorporation of inorganic fillers into polymers. Among these fillers, an attractive alternative to conventional ones as reinforcement of polymers[1–5] seems to be ash and fly ash produced from carbon and other fossil fuels combustion. They are cheaper than their synthetic counterparts and allow reusage of the industrial wastes, which is also a goal of current industries mainly driven by existing environmental rules and regulations. The fly ash is not only used as filler but also value-added products as cordierite ceramic for thermal applications,[6] heat and sound insulation sandwich panels,[7,8] and floor and wall tiles.[7] Lightweight concrete is the another main fly ash application as reinforcement.[9]

On the other side, vinylester is a thermosetting polymer with very good chemical resistance, thermal stability, and mechanical strength.[10] In addition, its low viscosity makes it very attractive for liquid composite molding techniques. However, vinylester has low ductility and poor fracture toughness, which limits its applications as engineering material.[11]

The most widely used methods to toughen thermosetting resins are the incorporation of rubber or inorganic particles.[12] Rubber toughening can lead to a significant increase in toughness, but this method usually leads to a decrease in the material stiffness and strength, which may be undesirable in many applications. Toughening from inorganic fillers, on the other hand, could result in a more modest improvement of toughness but without significant loss of strength and even with an improvement in modulus.[12,13]

With the use of inorganic fillers, the most important toughening mechanisms have been proposed to be microcracking and crack pinning.[13] Other energy-absorbing mechanisms such as debonding/diffuse matrix shear yielding, step formation, and microshear banding have also been reported for glass bead-filled epoxies.[12,14] However, the toughening of thermosets by means of inorganic particles has been shown to be very complicated,[12] and some aspects of it still appear controversial in the literature.[13]

In the particular case of vinylester reinforced with fly ash, recently Ray et al.[15–17] reported the mechanical, thermal, and electrical properties of composites with relatively high filler contents (30–60 wt % ash). They focused their research mostly on

conventional properties such as flexural properties and dynamic–mechanical analysis.

The aim of this work was to study the deformation and fracture behaviors of composite materials based on a commercial vinylester resin reinforced with an industrial waste, fly ash, with special emphasis in the toughening mechanisms operative in these materials. The effect of filler content on those behaviors was also analyzed.

EXPERIMENTAL

Fly ashes kindly supplied by Industrias del Tablero S.A. (INTASA, Spain) were used as reinforcement. They were obtained from the biomass combustion and subsequently separated using a sieve of 250 mesh. Filler particle size distribution was obtained from scanning electron microscopy (SEM) micrographs of ash particles. Quantitative image analysis was performed with the help of the image processing software Image J. To ensure statistical validity of the analysis, a minimum of 250 particles was measured. The specific surface area of the filler was determined by the water-vapor adsorption method.[18]

The matrix material was prepared from general purpose vinylester resin (Derakane Momentum 411-350 from Dow, kindly provided by Poliresinas San Luis, Buenos Aires, Argentina) and methyl ethyl ketone peroxide as catalyst and cobalt naphthenate (CoNap) as accelerator.

Composites with different ash contents, 10, 20, 30, and 40 wt %, were prepared using the following procedure. The components (matrix and filler) were stirred in an ultrasonic bath at room temperature. The mixtures were immediately poured into molds to prepare the specimens to be used in the mechanical characterization.

Plaques (thickness, $B = 3$ and 5 mm) and cylinders of 6.5-mm diameter were obtained by casting the mixtures into molds (consisting of two rectangular glass plaques covered by a thin Teflon® layer, spaced by a Teflon® spacer and held together with clamps) and polyethylene tubes, respectively. The different mixtures of vinylester and filler were cured with the catalyst and CoNap as accelerator in weight fraction of 1 and 0.5%, respectively, at room temperature. Then, all plaques and tubes were postcured for 2 h at 140°C in an oven to reach full vinylester groups conversion. The cured plates and tubes were slowly cooled down to room temperature and removed from the mold to be machined to produce rectangular bars and cylinders for mechanical testing.

Filler volume fractions were calculated from the known weight fractions using the experimental density of the components (vinylester = 1.14 g/cm^3 and fly ash = 2.23 g/cm^3) measured by pycnometry following ASTM D 762-00 standard recommendations.

Glass transition temperatures, T_g, for the different materials were measured using differential scanning calorimetry (DSC) in a Perkin Elmer Pyris 1DSC analyzer. Samples of 12 mg were heated from room temperature up to 160°C at a rate of 10°/min. (The DSC equipment is periodically calibrated with indium standards to warrant the accuracy of the results.)

Uniaxial tensile tests were carried out in an Instron dynamometer 4467 equipped with a 30 kN load cell at 1 mm/min crosshead speed in accordance with ASTM D 638M-91 standard recommendations. A series of six rectangular specimens of 3 × 10 × 80 mm^3 were used. Gage length used was 12.7 mm. Stress–strain curves were obtained from these tests, and Young's modulus and tensile strength values were determined from these curves.

Uniaxial compression tests were also performed on cylindrical specimens cut out from the molded cylinders (diameter $D =$ 6.5 mm and height $H = 10$ mm) in the Instron dynamometer at 1 mm/min, in accordance with ASTM D 695M-91 standard. Compressive modulus and yield strength values were determined from the true stress–strain curves obtained in these tests. A series of six samples were tested.

Single-edge notched bend (SENB) specimens were cut out from thick plaques ($B = 5$ mm). Sharp notches were introduced by sliding a fresh razor blade into a machined slot. Nominal crack-to-depth (a/W) was $0.45 < a/W < 0.5$, nominal thickness-to-depth (B/W) and span-to-depth (S/W) ratios were always kept equal to 0.5, 0.5, and 4, respectively, in accordance with ASTM D 5045 standards.

Fracture characterization was carried out in three-point bending in the Instron dynamometer at 1 mm/min. Critical stress intensity factor (K_{IC}) values and energy release rate (G_{IC}) values were obtained independently from the critical load and the area under the load–displacement curve up to that load, respectively, following ASTM D 5045-93 standard recommendations.

Fracture surfaces of specimens broken in tensile and fracture tests were also analyzed by SEM (model JEOL JSM 6460 LV, Japan) after they had been coated with a thin layer of gold. Energy-dispersive X-ray spectroscopy (EDS) was also performed on the fracture surfaces of tensile specimens.

Fourier transform infrared (FTIR) analysis was also performed for the vinylester matrix, fly ash, and the composite with 40 wt % ash in a Nicolet 6700 spectrometer. The resolution was 4 cm^{-1}, and the range used was 4000–600 cm^{-1}.

Average surface roughness values (R_a) of the fracture surfaces obtained in three-point-bending fracture tests were measured by profilometry.

Theoretical Models for Composite Properties

Models for the Composite Modulus. Many theoretical models can be used to predict the modulus of particle-modified polymers. Although numerical modeling of the mechanical properties of a particulate-reinforced composite is possible by finite-element method, the detailed modeling of the properties is beyond the aim of this work. Effective and simple models allow, through parametric investigations, capturing the essentials of the structural behavior of a composite. Effective modulus theories based on homogenization techniques are developed for this purpose.

In this work, Halpin–Tsai[19–21] and Lewis–Nielsen models[20,22] were applied to predict the tensile and compressive modulus of our composites.

The Halpin–Tsai model gives the modulus of the material as a function of the modulus of the filler and the matrix and a shape factor ξ, as follows:

$$E_c = (1 + \xi\eta V_f)/(1 - \eta V_f)E_m \quad (1)$$

$$\eta = (E_f/E_m - 1)/(E_f - E_m + \xi), \quad (2)$$

where E_c, E_m, and E_f are the modulus of the composite, matrix, and filler, respectively, V_f is the volume fraction of the filler, and ξ is a shape factor ($\xi = 2w/t$, w is the particle length and t is the thickness). For spherical shape, aspect ratio (w/t) is 1; therefore, a value of $\xi = 2$ can be assumed in the calculations.

The predictions of the Halpin–Tsai model frequently overestimate experimental data of modulus[22] because of the assumption of perfect bonding between matrix and filler, which usually does not verify. To consider this effect, Lewis and Nielsen proposed the following prediction for the composite modulus:

$$E_c = [1 + (k_E - 1)\beta V_f/(1 - \beta\mu V_f)E_m, \quad (3)$$

where k_E is the Einstein coefficient, and β and μ are constants that take into account the ratio between the modulus of the filler and the matrix (E_f/E_m) and the maximum packing fraction (V_{max}), respectively:

$$\beta = (E_f/E_m - 1)/[E_f/E_m + (k_E - 1)] \quad (4)$$

$$\mu = 1 + (1 - V_f)/V_{max}[V_{max}V_f + (1 - V_{max})(1 - V_f)]. \quad (5)$$

For random close packing, nonagglomerated spheres with a value of $V_{max} = 0.632$ can be used. The value of k_E changes with the degree of matrix to particle adhesion[20,22] from 2.167 for the case with no interfacial slip and 0.867 for the slippage case assuming a value of Poisson's ratio $v = 0.35$.[22]

Models for the Composite Energy Release Rate. By considering the changes in properties due to the interaction between components proportional to the actual values of those properties, Pukánszky and Maurer[23] derived the dependence of fracture resistance on composition as follows:

$$G_{IC} = G_{ICm}(E_m/E)(1 - v_f)/(1 + 2.5v_f)\exp(B_{Gc}v_f). \quad (6)$$

The term E_m/E accounts for the inverse correlation between the stiffness and the fracture resistance of the material. The change in the effective load-bearing cross section of the matrix due to the presence of the filler is represented by $(1 - V_f)/(1 + 2.5V_f)$. The parameter B_{Gc} is related to the matrix–filler interface and is particularly unique for each system.

If the reduced properties are plotted against filler content in the linearized form of eq. (6), the effect of the reduced load-bearing cross section can be eliminated.

$$\ln G_{ICred} = \ln G_{ICm} + B_{Gc}v_f. \quad (7)$$

From the slope of the linear regression of experimental data, B_{Gc} can be determined and its value can be used to obtain the effect of component interaction on fracture resistance.

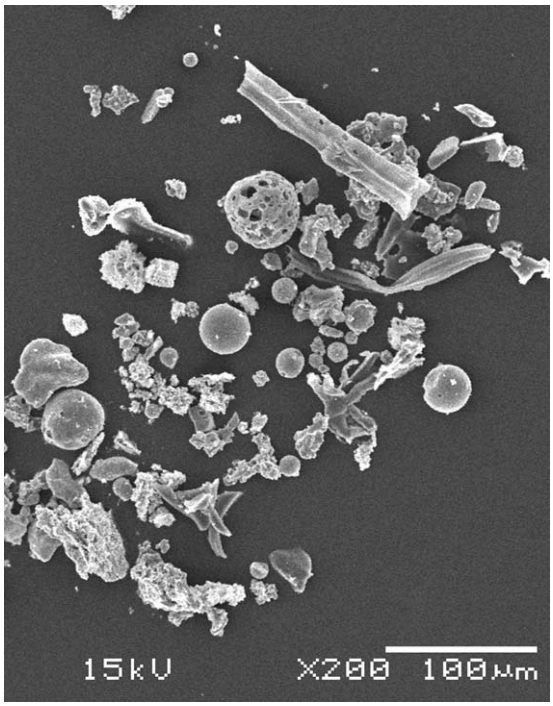

Figure 1. SEM micrograph of the fly ash particles.

Fly Ash Characterization. The ash particles used in this study are cenospheres, which consist of hollow particles containing a central porosity as well as porosity in the walls.[24] Figure 1 shows a SEM micrograph of the particles used. Although many ash particles appear very irregular, the mean radius was assumed to be the characteristic geometric dimension.

Figure 2 presents the particle size distribution of ash. The mean value was 25.38 μm with a standard deviation of 13.82 μm.

As it can be observed in this figure, a unimodal distribution of ash particles exists with a mean value between 10 and 20 μm. In addition, about 40% of the particles has radius within this range and about 20% of the particles has radius between 0 and 10 μm, 20% between 20 and 30 μm, and 20% greater than 30 μm.

X-ray diffraction (XRD) analysis was carried out to investigate crystal phases and composition of fly ash particles. A Phillips PW 1050/25 diffractometer operating in a 2θ range between 5° and 70° was used. The scattering angle was varied in 1°/min steps. CuKα radiation was used as source. General information of the fly ash is presented in Table I.

The results of this analysis are presented in Figure 3 where sharp peaks can be identified as quartz (SiO_2) and kyanite (Al_2SiO_5). It was assumed that the crystalline phase of fly ash consists only of these two elements (all other peaks are significantly lower in intensity). Calculation of the crystalline to glassy phase ratio was possible by comparing the areas of the broad glassy peak to sharp crystalline peaks, after subtracting the background intensity. Furthermore, by comparing the peak heights between the fly ash and the XRD results for a pure quartz sample, an estimation of the weight fraction of quartz in fly ash

Applied Polymer SCIENCE

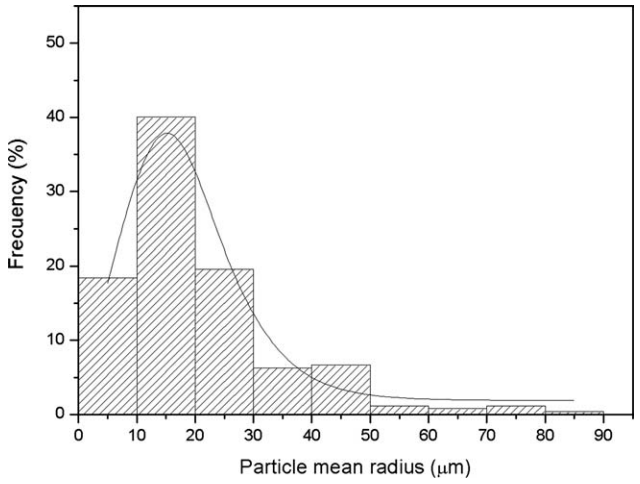

Figure 2. Particle size distribution of ash.

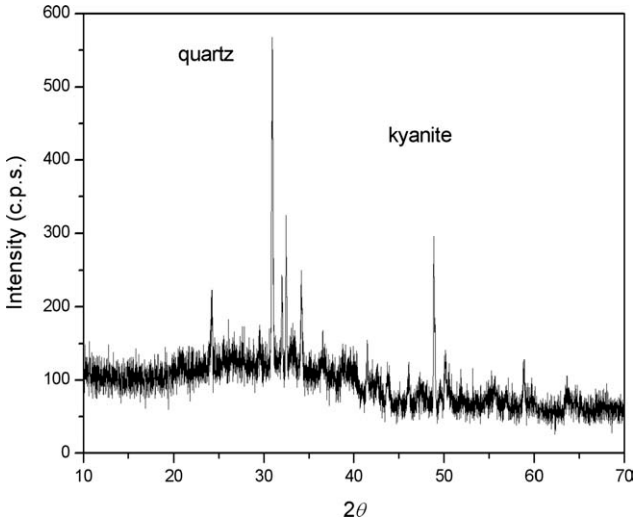

Figure 3. XRD pattern for ash.

was carried out. The volume fractions of the crystalline and glassy phases were calculated assuming a density of 2.65 g/cm^3 for quartz, 3.58 g/cm^3 for kyanite, and 2.5 g/cm^3 for the glassy phase.[25] The total glassy phase was found to be 80.3%, and the volume fractions of quartz and kyanite were 2.7 and 17.0%, respectively.

RESULTS AND DISCUSSION

Glass Transition Temperatures

Glass transition temperatures obtained from DSC are presented in Figure 4. As it can be observed in this figure, the T_g of the vinylester resin was increased by the presence of ash and also with ash content. The formation of an immobilized layer of polymer around rigid particles has already been reported in different composites. The presence of this layer is expected to increase the glass transition temperature (T_g) of the polymer matrix and/or broaden its dynamic mechanical peak.[22] Therefore, in our composites, the formation of an interphase of polymer around ash particles would have contributed to the increase in the vinylester glass transition temperature observed. In general, when particles are added to thermosetting resins, the amount of interphase increased as the dispersion of the particles is enhanced and their size is reduced. This is more evident when polymers are reinforced with nanofillers such as nanoclays or carbon nanotubes, which have large surface area. In the first case, it has been reported that small amounts of clay can immobilize a large amount of polymer chains[26,27] increasing storage modulus and glass transition of the composites. In the case of carbon nanotubes, Ramanathan et al.[28] showed that the same amount of filler (1%) can generate an important increase in T_g or have no effect in glass transition depending on the degree of dispersion (high degree of dispersion was achieved by functionalizing carbon nanotubes). When adding micrometric particles, the increase of the interphase region with lower polymer chains mobility, achieved when the degree of dispersion is increased, is expected to be less significant because of the lower surface area of the particles. In this work, an increase of more than 10% in T_g was observed when increasing the particle volume fraction from 0 to 0.25. In this case, the T_g can also be affected by the influence of the filler on the curing process of the vinylester resin. To obtain information about this process,[29] FTIR analysis was performed for vinylester, fly ash, and the composite with 40 wt % ash as an example. The corresponding spectra are presented in Figure 5.

Vinylester crosslinking reaction is the result of different kinds of reactions between the unsaturated double bonds: (i) vinylester

Table I. General Information of the Fly Ash Particles Studied

Property	Value
Mean radius	25.38 ± 13.82 μm
Density	2.23 g/cm^3
Glassy phase (vol %)	80.30%
Total crystalline phase (vol %)	19.7% (2.7% quartz and 17% kyanite)

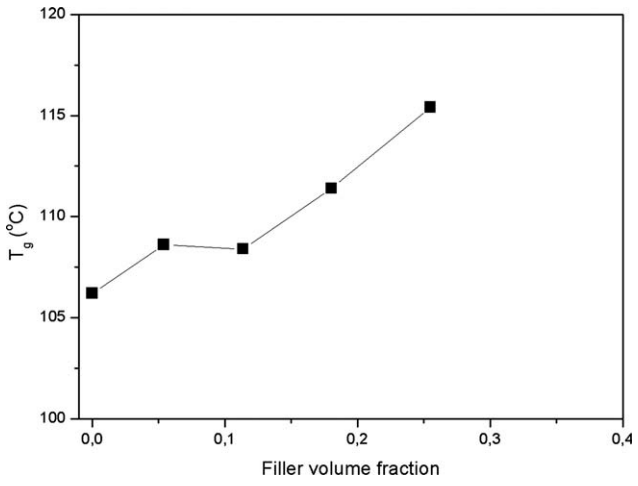

Figure 4. Glass transition temperature values for the different composites investigated.

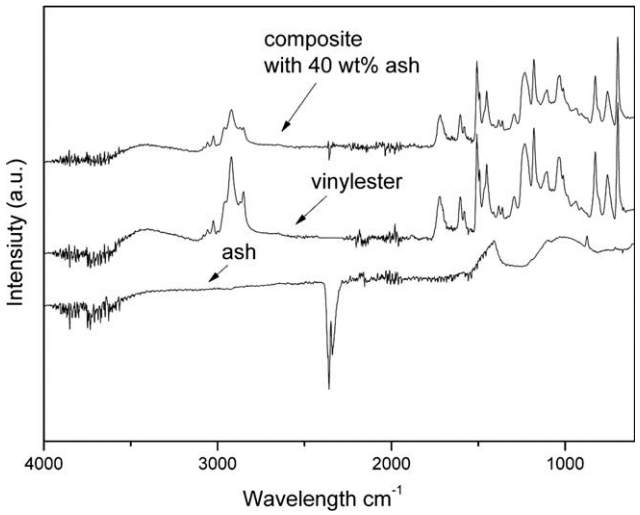

Figure 5. FTIR spectra for the vinylester matrix, fly ash, and the composite with 40 wt % ash.

prepolymer reacts with styrene, (ii) homopolymerization of styrene monomer giving polystyrene, and (iii) homopolymerization of the resins. The unreacted double bonds of the vinyl groups in the vinylester molecules and the styrene monomer can be detected by following the peaks at 930 and 898 cm^{-1}, respectively. There are also peaks at 830 and 700 cm^{-1} associated to the bending of aromatic carbon–hydrogen bonds of vinylester and styrene that can be used to correct the effects associated with evaporation and dimensional changes. In a previous work,[30] we observed that the microstructure developed during the curing processes could be characterized by the absorbance ratio of vinylester/styrene double bonds (930/898) normalized to the aromatic carbon–hydrogen double bonds. When this parameter increases (for example, by increasing the styrene content or changing the curing parameters), the microstructure goes from big highly crosslinking microgels to small microgels with lower crosslinking density. The value of the parameter obtained in this work for the 40 wt % fly ash/vinylester composite is 1.70, which is similar to the value of 1.81 obtained for the same unfilled resin in our previous work,[30] indicating that no significant effect of fly ash on the vinylester curing process exists. Therefore, the observed increase in the T_g with fiber loading could be mostly attributed to the formation of an immobilized layer of polymer around the ash particles rather than to an effect of the presence of fly ash on the vinylester curing process.

Deformation Behavior

All materials exhibited fully brittle behavior under tensile loading, whereas under uniaxial compression, ductile behavior characterized by the initial linear elastic response followed by yielding, strain softening, and strain hardening was always observed. In uniaxial compression tests, the stress is compressive and plastic yielding can occur for materials that under other conditions exhibit a brittle behavior,[31] such as the vinylester matrix and the composites investigated here.

Tensile (Young's modulus and tensile strength) and compressive (modulus and yield strength) parameters values normalized to the matrix values as a function of filler volume fraction are presented in Figure 6(a,b), respectively.

As it can be observed in Figure 6(a), Young's modulus values increased with filler content in agreement with expectations from the incorporation of a stiffer second phase in the vinylester matrix.[32,33] On the other hand, tensile strength initially increased for 10 wt % fly ash (5.4 vol %) and then a decreasing trend of ultimate strength with filler loading was found probably because of particle agglomeration (SEM micrographs are presented in fracture surfaces analysis section). However, most composites were stronger than the matrix. Different trends of the effect of particle loading on composite strength have been reported in the literature[34] as a result of the interplay between the most important determining factors of strength: particle size, particle/matrix interfacial adhesion, and particle loading.

Furthermore, a linear increase in the compressive modulus with ash content [Figure 6(b)] was observed up to 30 wt % ash (18 vol %) in agreement with tensile tests results. In contrast, a decreasing trend of compressive yield strength values with ash content was found [Figure 6(b)]. The higher scatter of experimental data of compressive parameters for the composite with the highest filler content (25.5 vol %) complicates the analysis of the results in this case.

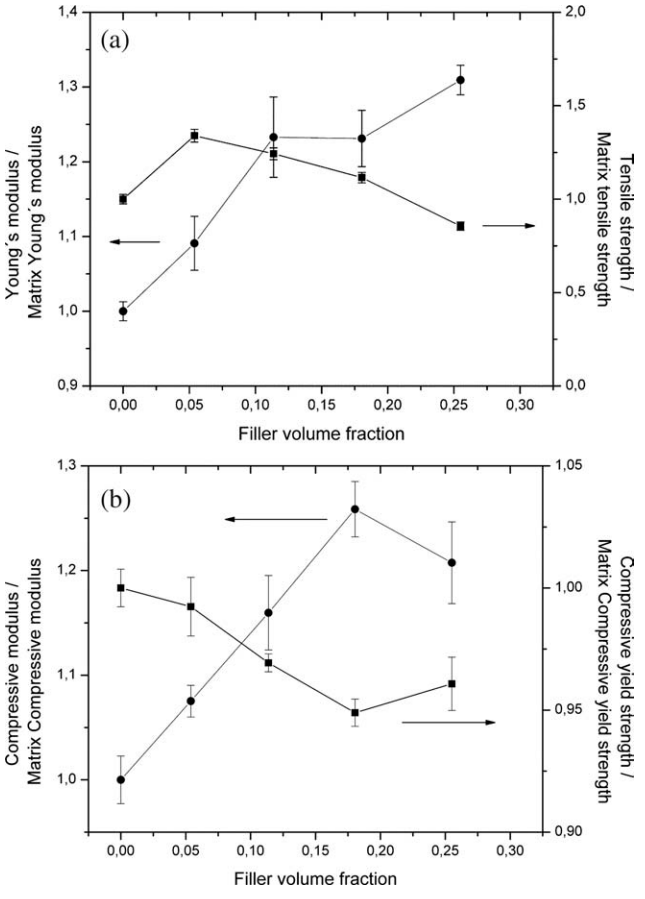

Figure 6. Tensile and compressive parameters values normalized to the matrix values as a function of filler volume fraction. (a) Young's modulus and tensile strength values. (b) Compressive modulus and yield strength values.

Applied Polymer SCIENCE

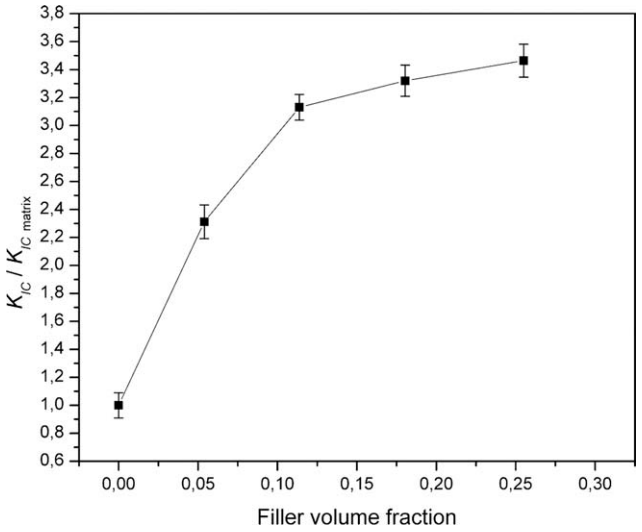

Figure 7. Critical stress intensity factor values normalized to the matrix value as a function of filler volume fraction.

It is important to note that a significant reinforcement effect was achieved from the incorporation of fly ash to vinylester, as most composites simultaneously exhibited higher stiffness and tensile strength values than the matrix.

Fracture Behavior

In fracture tests, the vinylester matrix and the composites displayed almost linear elastic behavior and failed by unstable crack growth. Therefore, single initiation values of the fracture parameters were obtained.

Critical stress intensity factor (K_{IC}) values and energy release rate (G_{IC}) values normalized to the matrix values are presented in Figures 7 and 8, respectively, along with their deviations. It can be observed in these figures that both K_{IC} and G_{IC} presented a maximum around 30 wt % ash (18 vol %). A maximum in the fracture toughness of glass-filled epoxy and polyester resins at a medium glass loading of about of 30% has already been reported in the literature.[29,34–36] As it will be mentioned later, the main contributions to toughness arise from out-of-plane processes related with matrix inelastic deformation localized around the particles. At higher filler content, fracture energy decreases because of the increase in the composite Young's modulus as well as because of the reduction of the proportion of matrix/filler and, consequently, of the amount of matrix able to undergo deformation. Therefore, fewer particles are effective as points of matrix yielding.[29]

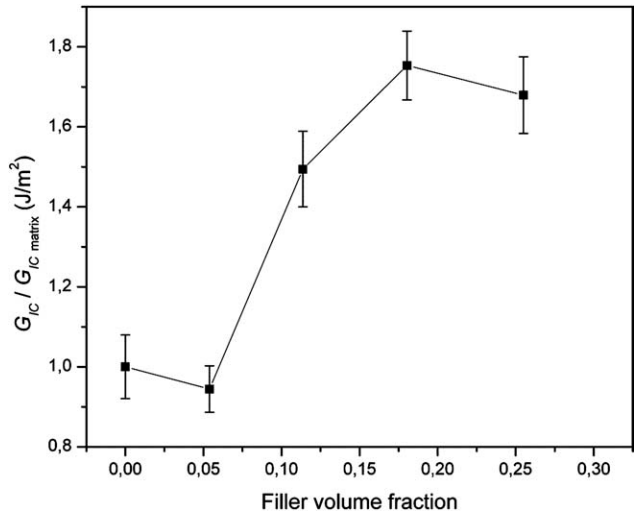

Figure 8. Critical energy release rate values normalized to the matrix value as a function of filler volume fraction.

Values of the critical stress intensity factor (K_{IC}) and the critical energy release rate parameter (G_{IC}) were obtained from load-displacement records. However, G_{IC} can also be calculated from fracture toughness values as follows:

$$G_{IC} = K_{IC}^2/E(1-\upsilon^2),$$

where E is the modulus of elasticity obtained from the tensile tests and υ is the Poisson's ratio of the polymer, taken to be 0.35.[17]

Table II shows the results of the above calculation.

As it can be clearly seen in Table II, there are differences among the calculated and the measured energy release rate parameter values being measured; values are always higher than calculated ones. This is probably because of the existence of some dissipation mechanisms such as plastic void growth and matrix plastic deformation that are not accounted in linear elastic fracture mechanics (LEFM). It should also be noted that all composites exhibited fracture toughness values significantly higher than that of the vinylester matrix, reaching an increase in K_{IC} as high as 250% for the composite with 40 wt % ash (25.5 vol %).

Fracture Surface Analysis and Toughening Mechanisms

SEM micrographs of the fracture surfaces of SENB specimens are shown in Figure 9 for the vinylester matrix and Figure 10(a,b) for the composite with 10 wt % ash. Typical features of the fracture of brittle unmodified thermosets[14] are clearly observed in Figure 9 for the vinylester matrix. They are characterized by relatively smooth and glassy fracture surfaces with no signs of large-scale plastic deformation.[22] Feather markings (i.e., apparent steps and changes of level of the crack) are also seen. They are caused by crack forking because of the excess of energy associated with the relatively fast crack growth in a brittle material. This is in agreement with the low value of fracture

Table II. G_{IC} Values Calculated from Fracture Toughness and Measured from Load-Displacement Records

	G_{IC} (J/m^2)	
Filler volume (%)	Calculated	Measured
5.39	378.76	487.81
11.37	643.71	771.75
18.04	667.37	905.63
25.5	757.17	867.33

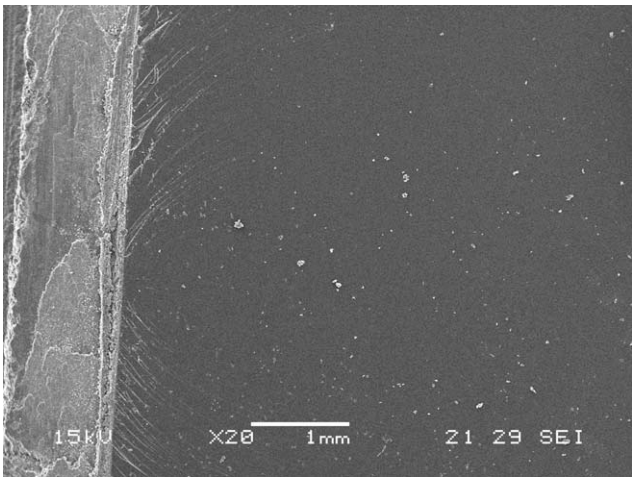

Figure 9. SEM micrograph of the fracture surface of a SENB specimen (×20) of the vinylester resin.

toughness obtained for the matrix ($K_{IC} = 0.47 \pm 0.09$ MPa $m^{1/2}$), which is typical of brittle polymers.[22]

In Figure 11, the progression in the degree of dispersion of the reinforcement in the matrix is presented. It was observed that for lower filler contents, ash particles are rather homogenously dispersed in the vinylester matrix. As the reinforcement content increases, the particles start to agglomerate. This is clearly observed for 40 wt % fly ash content [Figure 11(d)]. On the other side, pores are present in samples with higher ash contents. However, the volume of pores was measured by pycnometry, and it was found that the highest value of porosity did not exceed a value of around 8% for the composite with the highest filler content (40 wt % ash). These phenomena (particle agglomeration and increasing porosity) are responsible for the decrease of tensile strength for higher particle volume fractions.

It has been observed in the literature[22] that the addition of rigid particles to a brittle polymer leads to the development of different processes that can contribute to the overall toughness. These processes have been categorized as on-plane processes, such as crack bowing and crack deflection, and off-plane processes, such as debonding and plastic void growth and localized shear yielding.[29]

In the case of micron-sized filler particles that are much larger than the plastic zone size, the crack pinning mechanism is expected to occur.[22] It is identified by the presence of bowing lines on the fracture surface as the particles in a brittle matrix resist crack propagation by making the crack front bow out between particles.[14] Tails are caused by the two sections of the pinned crack joining up. More elastic energy is stored in the bowed secondary crack front than in the straight unbowed crack front. Hence, crack propagation requires more energy.[14]

In the SEM micrograph of Figure 10(b) [closer view of Figure 10(a)], the bowing marks characteristic of the crack pinning toughening mechanism are clearly observed (see arrows). Hence, this energy absorption mechanism existed in the composites investigated here.

Crack deflection should also be taken into account in our composites. In this mechanism, the crack front tilts and twists when it founds rigid particles and passes around them. Thus, it leads to an increase in the total fracture surface area and makes the crack to grow locally under mixed-mode conditions.[22] Under these conditions, crack propagation requires more energy dissipation than under mode I loading.[36] It has been established in the literature[22] that the toughening effect because of the increase in the true fracture surface area gives a linear relationship between the surface roughness and the overall toughening contribution, Ψ ($\Psi = G_{IC} - G_{ICm}$, where G_{IC} and G_{ICm} are the fracture energy for the composite and the matrix, respectively). In this work, the average surface roughness (R_a) was measured by profilometry, and their values were plotted as a function of the overall toughening contribution. Standard deviation for vinylester matrix and 10 wt % fly ash was 0.00896 and 0.08995, respectively, and is difficult to see in the figure. A nonlinear dependence of the average surface roughness with the overall toughening contribution was found (Figure 12), suggesting that the increase in the true fracture surface area was not uniquely responsible for the increase in toughness obtained.

In addition, although crack pinning and crack deflection were occurring in the composites investigated here, these mechanisms[14,37]

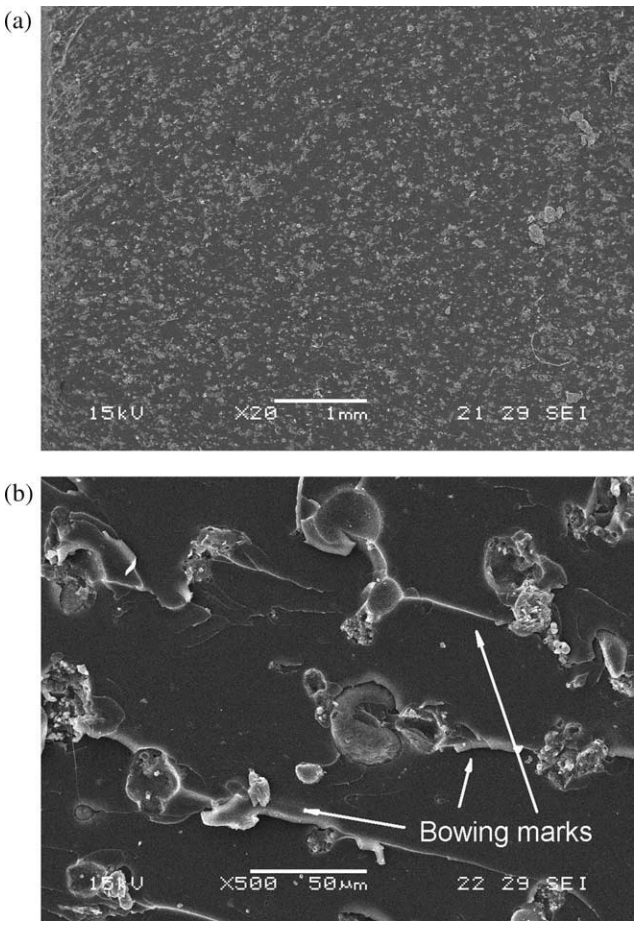

Figure 10. SEM micrographs of the fracture surface of a SENB specimen of the composite with 10 wt % ash. (a) ×20 and (b) ×500.

Applied Polymer SCIENCE

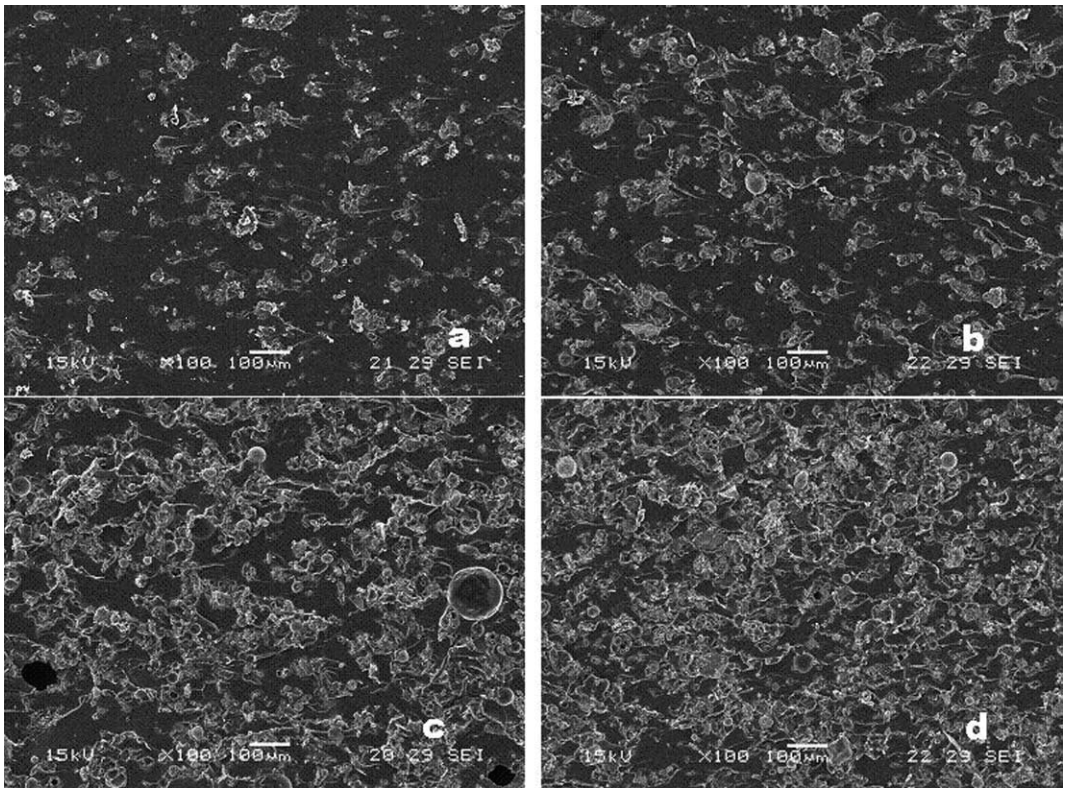

Figure 11. (a) SEM micrograph of the fracture surface of a tensile specimen of the composite with 10 wt % ash. (b) 20 wt % ash, (c) 30 wt % ash, and (d) 40 wt % ash.

are only relevant for significantly brittle materials such as ceramics and glasses. Their contribution to toughness is negligible against other toughening mechanisms (out-of-plane processes) related with matrix inelastic deformation localized around the particles.[29]

Debonding of the particles from the matrix as the crack advances, promoted by the triaxial tensile stresses acting at the crack tip, is another possible toughening mechanism in our composites. Although debonding generally absorbed little energy, it is essential because it reduces the crack tip constraint allowing the matrix plastic deformation to occur via a void growth mechanism[22] and/or the formation of shear bands.[14,22] Debonding at a matrix–particle interface is clearly observed in Figure 10(b). Therefore, this toughening mechanism was also occurring in the composites investigated.

In addition, some whitening in the vicinity of ash particles can also be observed in Figure 10(b), indicating the matrix inelastic deformation in the form of localized shear yielding. Small steps aligned in the crack propagation direction are also seen on the surface of vinylester. They arise from the existence of local shear stress during crack propagation.[29]

Furthermore, the presence of an immobilized layer of polymer around the particles mentioned before would have also contributed to the overall toughness.[22]

Figure 13(a,b) presents a SEM micrograph of a specimen of the composite with 30 wt % ash (18 vol %) broken in tension and the EDS spectrum in the vicinity of an ash particle, respectively, and Figure 14 is a close view of a fractured ash particle showing the typical cenosphere morphology. A free space between the ash particle and the matrix near the pole of the particle can be clearly seen in Figure 13(a), suggesting a relatively poor adhesion between both phases. However, as a result of the rather high specific surface area of ash (79 m^2/g), some amount of polymer adhered to the interphase could be expected[37] as well as mechanical interlocking due to the cenosphere morphology of ash consisting of hollow particles with a central porosity and

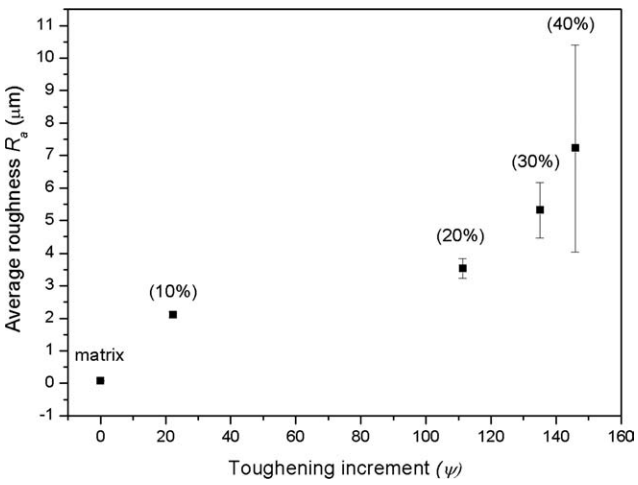

Figure 12. Average surface roughness as a function of the toughening contribution.

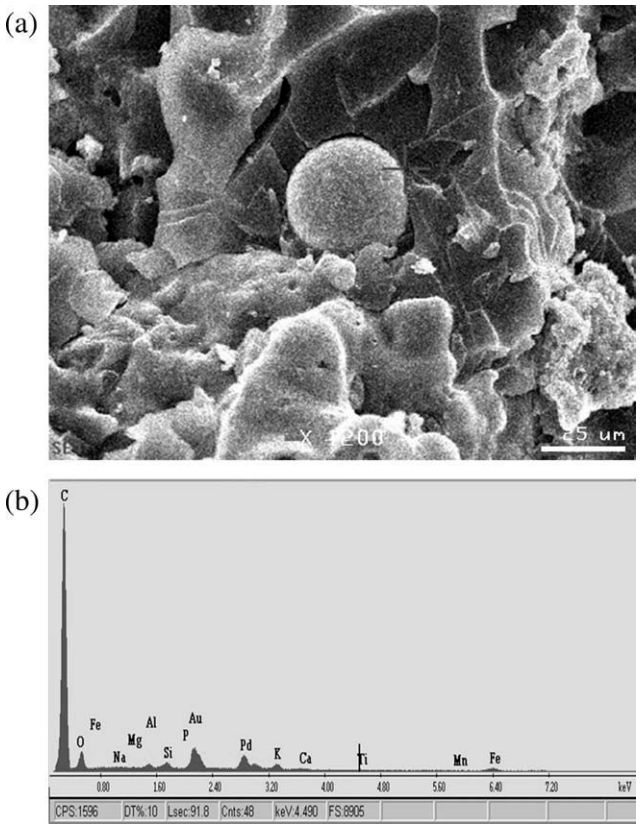

Figure 13. (a) SEM micrograph of the fracture surface of a tensile specimen of the composite with 30 wt % ash. (b) EDS spectrum.

porosity in the walls (Figure 14). In addition, in the EDS spectrum for the vicinity of the ash particle [Figure 13(b)], a small fraction of aluminum and silicon derived from the aluminum silicate of ash was found, indicating some kind of interaction between the polymer and ash.

From the above observations, it can be concluded that even if an interaction between phases existed, it was not very strong.

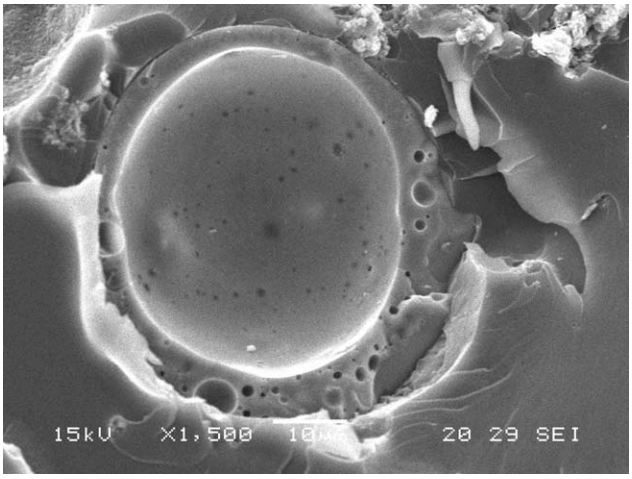

Figure 14. Close view of a fractured ash particle showing the typical cenosphere morphology.

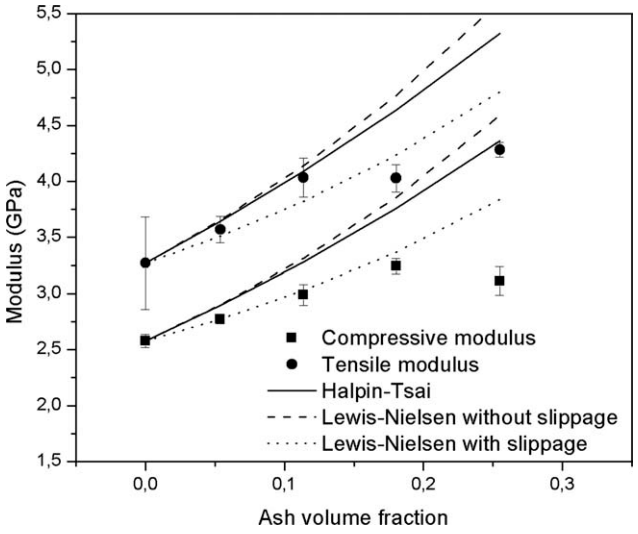

Figure 15. Experimental data of the tensile and compressive modulus versus ash volume fraction and theoretical predictions from Halpin–Tsai and Lewis–Nielsen models.

Modeling of the Composite Modulus

To make the calculations involved in the modeling of composite modulus, a reliable value of the modulus of ash was needed. It was estimated from the crystallinity and the volume fraction of each component in fly ash determined by XRD analysis.

For the estimation of the modulus of fly ash, the cenosphere morphology consisting of a hollow structure with central porosity and some porosity in the walls was considered, and the procedure of Matsunaga et al.[24] was used. A detailed description of this procedure has been previously reported in Refs. 24 and 38.

By introducing the estimated value of the cenosphere modulus (E_f = 24.01 GPa) in the Halpin–Tsai and Lewis–Nielsen models for the prediction of the modulus, the results presented in Figure 15 were obtained.

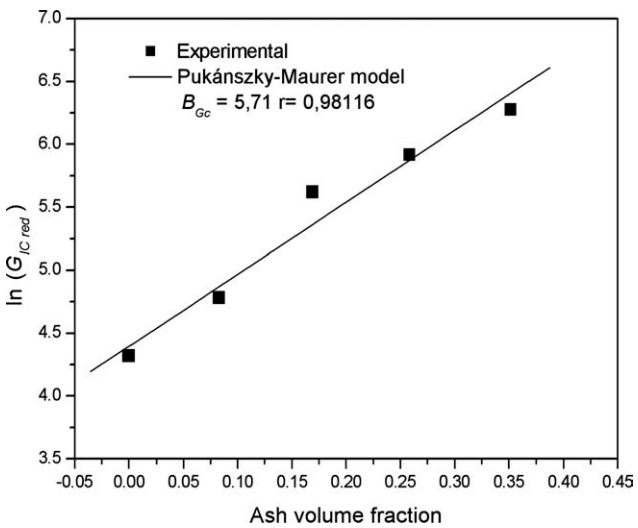

Figure 16. Pukánszky and Maurer model applied to experimental values of the energy release rate parameter for the vinylester/ash composites.

Experimental data of tensile and compressive modulus lie significantly below the predictions of the Halpin–Tsai and Lewis–Nielsen models without slippage. This indicates that even if some bonding between filler and matrix existed it was far from being perfect. On the other hand, the Lewis–Nielsen model with slippage reasonably fitted experimental data of the compressive modulus up to about 18 vol % ash. Therefore, some slippage was occurring at the interface in the composites investigated.

Modeling of the Composite Energy Release Rate

The results obtained from the application of Pukánszky and Maurer model to our composites are shown in Figure 16. A good linear correlation between experimental data of reduced G_{IC} values and ash volume fraction was obtained. The relative low value of the interaction parameter of fracture energy (B_{Gc}) would suggest that some interaction between both phases existed, in agreement with EDS analysis.

CONCLUSIONS

In this work, the deformation and fracture behaviors of a commercial vinylester resin reinforced with fly ash were investigated. Special emphasis was put in the identification of the toughening mechanisms operative in these materials.

Important improvements in the mechanical properties of materials were found from the incorporation of fly ash to vinylester, as most composites simultaneously displayed higher stiffness, tensile strength, and fracture toughness values than neat matrix.

The toughening mechanisms occurring in our composites were found to be crack bowing, crack deflection, the formation of an immobilized layer of polymer around ash, particle debonding, and localized shear yielding. All these mechanisms were observed to occur simultaneously with no significant preponderance of any of them.

From the application of simple models available in the literature for the prediction of composite stiffness and fracture energy, some interaction between filler and matrix was assumed to exist. This is in agreement with the results of EDS analysis around ash particles.

As a general conclusion, we can say that composite materials with simultaneously improved stiffness, tensile strength, and fracture toughness, based on a commercial thermosetting polymer and an industrial waste, could be obtained.

ACKNOWLEDGMENTS

The authors thank the National Research Council of Argentina (CONICET) for the financial support of this investigation.

REFERENCES

1. Bose, S.; Mahanwar, P. A. *J. Miner. Mater. Charact. Eng.* **2004,** *3*, 65.
2. Stefani, P. M.; Cyras, V.; Tejeira Barchi, A.; Vazquez, A. *J. Appl. Polym. Sci.* **2006,** *99*, 2957.
3. Stefani, P. M.; Garcia, D.; Lopez, J.; Jimenez, A. *J. Therm. Anal. Calorim.* **2005,** *81*, 315.
4. Chaudhary, D. S.; Jollands, M. C.; Cser, F. *Adv. Polym. Technol.* **2004,** *23*, 147.
5. Wang, M.; Shen, Z.; Cai, C.; Ma, S.; Xing, Y. *J. Appl. Polym. Sci.* **2004,** *92*, 126.
6. Kumar, S.; Singh, K. K.; Ramachandrarao, P. *J. Mater. Sci.* **2001,** *36*, 5917.
7. Kumar, R.; Kumar, S.; Mehrotra, S. P. *Resour. Conserv. Recycl.* **2007,** *52*, 157.
8. Bhattacharjee, U.; Kandpal, T. C. *Energy* **2002,** *27*, 151.
9. Kockal, N. U.; Ozturan, T. *Mater. Des.* **2011,** *32*, 2396.
10. Gryshchuk, O.; Karger-Kocsis, J.; Thomann, R.; Kónya, Z.; Kiricsi, I. *Compos. Part A: Appl. Sci. Manuf.* **2006,** *37*, 1252.
11. Robinette, E. J.; Ziaee, S.; Palmese, G. R. *Polymer* **2004,** *45*, 6143.
12. Lee, J.; Yee, A. F. *Polymer* **2001,** *42*, 577.
13. Kawaguchi, T.; Pearson, R. A. *Polymer* **2003,** *44*, 4239.
14. Lee, J.; Yee, A. F. *Polymer* **2000,** *41*, 8375.
15. Ray, D.; Banerjee, S.; Mohanty, A. K.; Misra, M. *Polym. Compos.* **2008,** *29*, 58.
16. Ray, D.; Bhattacharya, D.; Mohanty, A. K.; Drzal, L. T.; Misra, M. *Macromol. Mater. Eng.,* **2006,** *291*, 784.
17. Ray, P. K.; Mula, S.; Mohanty, U. K.; Ray, B. C. *J. Reinf. Plast. Compos.* **2007,** *26*, 519.
18. Smith, D.; Green, H. *Ind. Eng. Chem. Anal. Ed.* **1942,** *14*.
19. Ahmed, S.; Jones, F. R. *J. Mater. Sci.* **1990,** *25*, 4933.
20. Stapountzi, O. A.; Charalambides, M. N.; Williams, J. G. *Compos. Sci. Technol.* **2009,** *69*, 1677.
21. Halpin, J. C.; Kardos, J. L. *Polym. Eng. Sci.* **1976,** *16*, 344.
22. Johnsen, B. B.; Kinloch, A. J.; Mohammed, R. D.; Taylor, A. C.; Sprenger, S. *Polymer* **2007,** *48*, 530.
23. Pukánszky, B.; Maurer, F. H. J. *Polymer* **1995,** *36*, 1617.
24. Matsunaga, T.; Kim, J. K.; Hardcastle, S.; Rohatgi, P. K. *Mater. Sci. Eng. A* **2002,** *325*, 333.
25. Chung, F. *J. Appl. Crystallogr.* **1974,** *7*.
26. Rao, Y. Q.; Pochan, J. M. *Macromolecules* **2007,** *40*, 290.
27. Kaushik, A. K.; Podsiadlo, P.; Qin, M.; Shaw, C. M.; Waas, A. M.; Kotov, N. A.; Arruda, E. M. *Macromolecules* **2009,** *42*, 6588.
28. Ramanathan, T.; Liu, H.; Brinson, L. C. *J. Polym. Sci. Part B: Polym. Phys.* **2005,** *43*, 2269.
29. Sánchez-Soto, M.; Pagés, P.; Lacorte, T.; Briceño, K.; Carrasco, F. *Compos. Sci. Technol.* **2007,** *67*, 1974.
30. Rodriguez, E.; Larrañaga, M.; Mondragón, I.; Vázquez, A. *J. Appl. Polym. Sci.* **2006,** *100*, 3895.
31. Arias, M. L.; Frontini, P. M.; Williams, R. J. J. *Polymer* **2003,** *44*, 1537.
32. Auad, M. L.; Frontini, P. M.; Borrajo, J.; Aranguren, M. I. *Polymer* **2001,** *42*, 2723.
33. Százdi, L.; Pozsgay, A.; Pukánszky, B. *Eur. Polym. J.* **2007,** *43*, 345.
34. Fu, S.-Y.; Feng, X.-Q.; Lauke, B.; Mai, Y.-W. *Compos. Part B: Eng.* **2008,** *39*, 933.
35. Broutman, L. J.; Sahu, S. *Mater. Sci. Eng.* **1971,** *8*, 98.
36. Johnsen, B. B.; Kinloch, A. J.; Taylor, A. C. *Polymer* **2005,** *46*, 7352.
37. Móczó, J.; Pukánszky, B. *J. Ind. Eng. Chem.* **2008,** *14*, 535.
38. Stocchi, A. PhD Thesis. **2007**, Mar del Plata, Argentina.